

An Idealized Comparison of One-Way and Two-Way Grid Nesting

LUCAS M. HARRIS* AND DALE R. DURRAN

DEPARTMENT OF ATMOSPHERIC SCIENCES

UNIVERSITY OF WASHINGTON, SEATTLE, WASHINGTON

November 23, 2009

*Corresponding Author Address: Lucas Harris, Department of Atmospheric Sciences, Box 351640, University of Washington, Seattle, WA, 98105. E-Mail: lharris@atmos.washington.edu.

ABSTRACT

Most mesoscale models can be run with either one-way (“parasitic”) or two-way (“interactive”) grid nesting. This paper presents results from a linear 1D shallow-water model to determine whether the choice of nesting method can have a significant impact on the solution. Two-way nesting was found to be generally superior to one-way nesting. The only situation in which one-way nesting performs better than two-way is when very poorly-resolved waves strike the nest boundary. A simple filter is proposed for use exclusively on the coarse-grid values within the sponge zone of an otherwise conventional sponge boundary condition. The two-way filtered sponge BC gives better results than any of the other methods considered in these tests. Results for all wavelengths were found to be robust to other changes in the formulation of the sponge boundary, particularly with the width of the sponge layer.

The increased reflection for longer-wavelength disturbances in the one-way case is due to a phase difference between the coarse- and nested-grid solutions at the nested-grid boundary that accumulates because of the difference in numerical phase speeds between the grids. Reflections for two-way nesting may be estimated from the difference in numerical group velocities between the coarse and nested grids, which only becomes large for waves that are poorly-resolved on the coarse grid.

1. Introduction

Nested grids are extensively used in numerical modeling of the atmosphere for a wide range of applications, including numerical weather prediction (Mass et al. 2002), mesoscale meteorology, regional climate modeling (Giorgi and Mearns 1999), and air quality modeling (Krol et al. 2005). The implementation and proper use of grid nesting requires attention to intergrid communication, which can be split into two different problems.

The first part is communication from the coarse grid to the nested grid, typically through the specification of the boundary conditions (BCs) of the nested grid. The conditions at

the nested grid boundary must satisfy the radiation condition that outgoing disturbances should leave the nested grid without causing reflections back into the domain, but also allow disturbances on the coarse grid to propagate onto the nested grid without distortion. Several such BCs are reviewed in Zhang et al. (1986) and Staniforth (1997).

The second part of the grid communication problem is that from the nested to the coarse grid, also referred to as coarse-grid updating. Many mesoscale models give the choice of either one-way (parasitic) nesting or two-way (interactive) nesting. One-way nesting performs no nested-to-coarse grid communication; the solution on the coarse grid is simply independent of that on the nested grid. On the other hand, in two-way nesting the solution on the coarse grid is continually replaced (or “updated”) by that on the nested grid wherever the two grids coincide. A number of update algorithms have been proposed; see Zhang et al. (1986) and Skamarock and Klemp (1993) for some examples.

Admonitions to use two-way nesting are occasionally seen in the literature (Warner et al. 1997; Clark and Farley 1984; Phillips and Shukla 1973), but the few examples given supporting this assertion do not show a dramatic difference between one- and two-way nesting, and one-way nesting is still used in some applications (Mass et al. 2002; Colle et al. 2005; Deng and Stull 2005) and in some operational forecasts (Table 1). Warner et al. (1997) note that the potential improvements of two-way nesting have not been confirmed by research. Elsberry (1978) discusses potential problems with one-way nesting, but neither tests nor quantifies these problems with numerical experiments. Sundstrom and Elvius (1979) claim that two-way nesting may give larger errors than one-way nesting due to reflections caused by the change of phase speeds between the nested and coarse grids. However, they also do not give any examples supporting this assertion, and furthermore do not consider similar effects when using one-way nesting.

Phillips and Shukla (1973) compared the reflections of nonlinear, two-dimensional shallow-water Rossby and gravity waves off of the interface of both one-way and two-way nested grids. They found that the solutions for a two-way nest were “almost invariably nearer” to a single-

grid control case with the same resolution as the nested grid. However, they did not give any rigorous explanation for this beyond the basic fact that the coarse grid solution is influenced by that of the nested grid over the region on which the two grids coincide.

Clark and Farley (1984) performed a one-way simulation of vertically-propagating mountain waves that was considerably noisier than the same simulation performed with a two-way nest, but the majority of the errors in their one-way nest appeared to be due to reflections off of the nested grid's upper boundary, which did not coincide with the coarse grid's upper boundary. This type of vertical nesting is not used in most mesoscale models.

Vichnevetsky (1981) analyzed the reflections that occur as a wave propagates through a grid refinement, which as we shall see is relevant to the problem of two-way nesting. He found that the reflection coefficient, or the ratio of the amplitudes of the incident and reflected waves, can be determined through a simple expression involving the discrete group velocities on either side of the refinement. Mar-Or and Givoli (2006) carefully analyzed reflections in the 1D linear shallow-water equations using the Carpenter (1982) BC at the edge of a one-way nest, but they did not consider two-way nests or a wider range of practically important boundary conditions.

In this paper, we examine the reflection of a localized disturbance exiting the nested grid for both one- and two-way nests using either of a pair of common nested-grid BCs: simple interpolation and a Davies (1976) sponge layer, as well as a simple modification to the latter which has the potential to greatly decrease spurious reflection for poorly-resolved solutions. Although the interpolation BC is not particularly effective at eliminating reflections, we consider it because it allows for a simple analysis of the amplitude of reflections at the nested-grid boundary. For the same reason, we will use a simple one-dimensional model whose behavior can be rigorously analyzed without undue complication. Our goal is to determine whether one of the nesting strategies is superior, and why. A forthcoming paper will describe the differences between one- and two-way nesting in complex meteorological flows.

Section 2 of this paper describes the 1D model used and the experiments carried out. Section 3 presents results from the model. Section 4 compares the observed reflection amplitudes to theoretically derived results for the interpolation BC. Section 5 discusses the generality of the results. Section 6 concludes the paper.

2. Model Description and Methodology

The one-dimensional linear shallow-water model is described by the equations:

$$\frac{\partial u}{\partial t} + g \frac{\partial h}{\partial x} = 0 \quad (1)$$

$$\frac{\partial h}{\partial t} + H \frac{\partial u}{\partial x} = 0 \quad (2)$$

for velocity u , perturbation interface height h , gravitational acceleration $g = 9.8 \text{ m s}^{-2}$, and mean water depth H , which is chosen to satisfy $\sqrt{gH} = c = 5 \text{ m s}^{-1}$, where c is the shallow-water wave speed. There is no mean flow, Coriolis, or topography in these experiments.

The equations are discretized on a staggered grid, using second-order centered differencing in space and leapfrog differencing in time:

$$\delta_{2t}u + g\delta_x h = 0$$

$$\delta_{2t}h + H\delta_x u = 0.$$

The finite difference operators above are defined by the expression

$$\delta_{nx}\phi(x) = \frac{\phi(x + n\Delta x/2) - \phi(x - n\Delta x/2)}{n\Delta x} \quad (3)$$

for x , and similarly for t .

The simulations in this paper all use a periodic coarse grid with a x -direction width L_{xc} of 16 km and a nested grid whose western boundary is at 5 km and whose width is $L_{xn} = 6 \text{ km}$,

unless otherwise specified. On the coarse grid, $\Delta x_c = 20$ m, and $\Delta t_c = 0.4$ s, giving a Courant number of $c\Delta t/\Delta x = 0.1$. Grid nesting is implemented with a 3:1 refinement in space and time, as in many widely-used mesoscale models, giving a nested-grid spacing of $\Delta x_n = 6.7$ m and timestep of $\Delta t_n = 0.13$ s. Numerical simulations with the Courant number halved to 0.05 give almost the same results (to within 4%), as do simulations integrated using the third-order Adams-Bashforth method (Durran 1991) with $c\Delta t/\Delta x = 0.1$. Thus, our simulations may be interpreted as isolating the effects the spatial discretization on the solution.

Two types of nested-grid BC are used. The first, called the “interpolation” BC, merely interpolates the coarse-grid data to the boundary points on the nested grid for all variables on each nested grid timestep. This is the simplest “open” boundary condition for nested grids allowing both outflow and inflow, and allows for comparatively simple analytic expressions for the reflection amplitude. However, this BC performs substantially worse than other nested-grid BCs used in recent mesoscale models. The second BC uses the sponge-layer formulation in the Weather Research and Forecasting (WRF) model’s Advanced Research WRF dynamical core (Skamarock et al. 2005) for nested grids as of version 2.1.1 (as quoted in Moeng et al. 2007), in which the outermost point of the nested grid is interpolated, and the solution for each variable on the next N points in from the boundary (collectively, the “sponge zone”) are given as:

$$\begin{aligned}\left.\frac{\partial u}{\partial t}\right|_n &= -g\frac{\partial h}{\partial x} + w_{1n}(u_c - u_n) - w_{2n}\Delta^2(u_c - u_n) \\ \left.\frac{\partial h}{\partial t}\right|_n &= -H\frac{\partial u}{\partial x} + w_{1n}(h_c - h_n) - w_{2n}\Delta^2(h_c - h_n)\end{aligned}\quad (4)$$

where n is the index of this grid point in the sponge zone (counting inward from the interpolated point), u_c represents data interpolated from the coarse grid to the same point as u_n , Δ^2 represents a diffusive smoother (three points in this 1D model, in which case

$\Delta^2 u_i = u_{i-1} - 2u_i + u_{i+1}$); and the weighting coefficients in (4) are given by¹

$$w_{1n} = \frac{W}{\Delta t} \left(\frac{1 + N - n}{N} \right) \quad n = 1, 2, \dots, N, \quad (5)$$

and $w_{2n} = 0.2w_{1n}$. The coefficient W in (5) is referred to in this paper as the “sponge weight”; WRF sets this to 0.1, which is the value we use unless otherwise specified. In this study, $N = 5$ unless otherwise stated. This follows the example of Moeng et al. (2007), who needed five points to get acceptable results for their two-way nested large eddy simulations of the planetary boundary layer. In contrast, WRF by default uses only three sponge points, although this can be changed by the user.

The implementation of the sponge BC uses explicit forward differencing to evaluate the sponge terms in (4). The Δt in the denominator of (5) cancels out when the timestep is taken, ensuring that the amount of effective dissipation performed during a timestep is independent of its length. In our test cases, the sponge zone is added to the ends of the domain, so that the size of the interior region is identical for both BCs. When using the interpolation BC, the u boundary points are specified directly from the coincident coarse-grid points, while the h boundary points, which do not coincide with coarse-grid points on this staggered grid, are linearly interpolated to from the coarse grid. Linear interpolation is also used for all boundary and sponge-zone points when the sponge BC is used. Tests with the interpolation BC showed little change in the amplitude of reflected waves to the choice of interpolation method.

In our simulations, the grids are aligned so that *all* of the coarse-grid points coincide with a nested-grid point, and so the additional step performed in two-way simulations of updating the coarse grid using the nested grid’s data is performed by setting the values on

¹The expression for the sponge weights in the WRF documentation is slightly different than that given in (5). The expression in Skamarock et al. (2005) produces a weight of zero for the innermost point of the sponge zone (called the “relaxation zone” in WRF), and so the true width of the sponge zone is one grid point less than that specified by the user. Here, we have altered the expression so that every point in the sponge zone has a nonzero weight, but that the weights are the same for the N sponge points as they would be if WRF was set to use $N + 1$ points.

the coarse-grid points to the values of the coincident nested-grid points. This differs from the approach used by Skamarock and Klemp (1993) and others, in which the update uses averages of nested-grid points. When the sponge BC is used, the sponge zone is not included in the update process.

The initial condition (IC) used here consists of a Gaussian-modulated sinusoidal wave of a given wavelength λ specified on the nested grid, and then updated to the coarse grid (regardless of whether one-way or two-way nesting is used). The value of $u(x, 0)$ is chosen so that there is a single eastward-moving wave and the westward characteristic is set to zero. The IC is thus:

$$h(x, 0) = \cos((x - x_0)k) \exp(-(x - x_0)^2/\sigma)$$

$$u(x, 0) = \frac{g}{c}h(x, 0),$$

where $x_0 = L_{xc}/2 = 8$ km, $k = 2\pi/\lambda$ is the wavenumber, and $\sigma = 5.333(\text{km}^2)$. An example IC is seen in Fig. 1a.

3. Simulation Results

a. Waves of intermediate wavelength on the coarse grid

We begin by considering waves that are moderately-well resolved on the coarse mesh and very well resolved on the fine mesh. Fig. 1 compares the behavior of one-way and two-way nesting, along with the performance of both interpolation and sponge BCs when a $\lambda = 36\Delta x_n$ shallow-water wave ($12\Delta x_c$ on the coarse grid) encounters the boundary of the fine mesh. The initial condition on the nested grid is shown in Fig. 1a. The next four panels show the solution at a time when it has propagated through the right boundary and any reflected wave has returned to the center of the nested grid. Clearly one-way (gray lines) nesting performs worse than two-way nesting (black lines), and the interpolation BC creates more reflection than the sponge. The amplitudes of the reflected waves shown in Fig. 1b–e are given as

percentage of their initial amplitudes in the first line of Table 2. These numerical values confirm the superiority of both two-way nesting and the sponge BC for this wavelength.

As shown by the next two lines in Table 2 the reflection becomes more severe as the wavelength is decreased, although for one-way nesting the increase is not a monotone function of the wavelength. In the one-way case, the reflections produced by the $18\Delta x_n$ wave are similar to those generated in the $36\Delta x_n$, while the behavior of the $24\Delta x_n$ is far worse. The reason the reflection for the $18\Delta x_n$ wave is reduced relative to that for the $24\Delta x_n$ wave will be discussed in Section 3a.

The behavior of the reflected modes in the shallow-water system is different from that produced at the nested grid boundary by numerical approximations to the 1D advection equation for a scalar concentration ϕ with constant background wind speed c ,

$$\frac{\partial\phi}{\partial t} + c\frac{\partial\phi}{\partial x} = 0.$$

If the preceding is discretized using leapfrog time differencing and second-order centered space differencing

$$\delta_{2t}\phi + c\delta_{2x}\phi = 0, \tag{6}$$

the only modes with negative group velocities, and therefore the only modes capable of transporting reflected waves away from the downstream boundary have wavelengths in the range $2\Delta x_n \leq \lambda < 4\Delta x_n$ (Durran 1999, Sec. 2.4.1). This is illustrated in Fig. 2 for one-way nesting, the interpolation BC, and an incident $36\Delta x_n$ wave packet moving at $c = 5 \text{ m s}^{-1}$. Fig. 2a shows the packet at the initial time, Fig. 2b shows the reflection after it propagates back to the center of the nested mesh as a high-amplitude mode of wavelength approximately $2\Delta x_n$.

Reflections into such short waves are easily removed by applying artificial dissipation.

Suppose fourth-order dissipation of the form

$$\frac{\gamma_4}{16\Delta t} (-\phi_{j-2} + 4\phi_{j-1} - 6\phi_j + 4\phi_{j+1} - \phi_{j+2}) \quad (7)$$

is added globally to the right-hand side of (6) when evaluating the value of ϕ_j at the next time level, where j represents the solution at $x = j\Delta x$. Using only a very weak dissipation coefficient (γ_4) of 0.01—an order of magnitude less than that used in many mesoscale models (cf. Knievel et al. 2007)—easily eliminates the reflected modes (Fig. 2c). For a $2\Delta x_n$ wave, this γ_4 yields an e-folding time for the wave amplitude of 53 s, or $0.017L_{xc}/c$. More generally, when reflections are comprised of very short wavelength modes, they will almost immediately be removed by the background dissipation present in nearly all mesoscale models.

On the other hand, in systems that support waves moving in both directions, such as the shallow-water equations, reflections often appear as spurious physical modes that are not easily removed by artificial dissipation because the magnitude of any artificial dissipation is normally set low enough that it does not significantly impact most physical modes. For example, adding significant dissipation (with $\gamma_4 = 0.1$) to the staggered shallow-water model and comparing the $36\Delta x_n$ case to that without dissipation, we see from Table 2 that even such relatively strong dissipation exerts only a modest influence on the amplitude of this very well-resolved reflected wave. This wave is damped with an e-folding time of approximately $7L_{xc}/c$, so there is very little reduction of the amplitude of either the incident wave or of the reflection; instead, the artificial dissipation is damping out the sharp discontinuity caused by the interpolation BC when the two solutions are out of phase, thereby reducing the amplitude of the reflected wave. Repeating this case with dissipation applied only at the two gridpoints nearest to the boundary yielded a reflection with a similar amplitude to a simulation with global dissipation, confirming this explanation.

Fig. 3a depicts the amplitude of the reflected wave as a function of the wavelength of the incident disturbance for the interpolation BC. Here, the reflections are given in terms of the

“normalized reflection amplitude”,

$$\frac{\max |h_{rn}|}{h_0} \quad (8)$$

where h_{rn} represents the value of $h(x, t)$ on the nested grid after the disturbance has been reflected and returned to the interior of the nested grid, and h_0 represents the initial amplitude of the outgoing disturbance. Again, the two-way nest (pluses) produces substantially lower-amplitude reflections than the one-way nest (crosses) for all but the shortest wavelengths. In fact, when using the interpolation BC the reflected wave’s amplitude for a $12\Delta x_n$ disturbance on a two-way mesh is roughly the same as that of a $48\Delta x_n$ disturbance on a one-way mesh! Using the sponge BC (Fig. 3b) reduces the errors in one-way nesting by as much as a factor of ten for some wavelengths, but one-way nesting still produces much larger reflections than does two-way nesting for wavelengths $\geq 12\Delta x_n$.

b. Poorly-resolved waves on the coarse grid

While for moderately-well resolved waves two-way nesting is superior, this is not the case for more poorly-resolved disturbances. When using the interpolation BC, the amplitude of the reflected wave is equal to that of the incident wave for wavelengths $\leq 9\Delta x_n$ for both one-way and two-way nesting (Fig. 3a). The sponge BC (Fig. 3b) again reduces the amplitude of the reflections for these short wavelengths, but is much more effective for one-way nesting than for two-way nesting.

The $9\Delta x_n$ case (Fig. 4a; see also Table 2) illustrates these behaviors. Using the interpolation BC (Fig. 4b), reflection is nearly total in the one-way case, and is only slightly reduced in the two-way simulation (Fig. 4c). Using the sponge BC, the reflected mode is substantially reduced with one-way nesting (Fig. 4d), but is almost half the amplitude of the incident wave in the two-way case (Fig. 4e). Although one-way nesting produces reflections of similar- or lower-amplitude than does two-way nesting for this $9\Delta x_n$ disturbance, the one-way results are degraded by a spurious mode propagating into the nested grid from the

outflow (right) boundary (Fig. 4bd).

The sudden shift in the behavior of the two-way nest’s reflections when the wavelength of the incident wave drops to $9\Delta x_n$ (Fig. 3) is surprising. One might expect disturbances to become “trapped” on the coarse grid and to produce total reflection only when the numerical group velocity of the wave on the coarse grid is directed inward. For our staggered-grid discretization of the shallow-water equations, we expect that trapping should only occur for wavelengths $\leq 6\Delta x_n$ (or equivalently, $\leq 2\Delta x_c$).

c. Filtered sponge BC: an improvement to the sponge BC

A close examination of the coarse-grid solution provides both a reason for this behavior as well as a solution. For poorly-resolved solutions, there is a substantial difference in the amplitudes and wavelengths of the solutions on the two grids, causing a mismatch between the solutions and thus larger reflections; in particular, in two-way nesting there can be a large difference in the wavelength of the fine-mesh solution and that on the coarse mesh outside the region where the grids overlap. If such short-wavelength waves are indeed causing the problems, then filtering the coarse grid data to remove the problematic high-frequency modes before using it in the sponge BC should decrease the amplitude of the reflections. To this end, we introduce the “filtered sponge” BC, in which the coarse-grid fields u_c and h_c are smoothed with the fourth-order filter (7) before being used in (4). Note that this filter is applied only to the data being used as the coarse-grid values in the sponge zone and does not alter the actual coarse-grid solution. Here, $\gamma_4 = 1$, so that any $2\Delta x_c$ waves are eliminated with a single pass of the filter. We use the fourth-order filter because it is a simple scale-selective filter that efficiently damps short wavelengths while having little effect on better-resolved disturbances.

The response of the filtered sponge BC to an incident $9\Delta x$ wave is compared with the other nested BCs in Fig. 4. In the one-way case, when the wave packet encounters the filtered sponge BC the filter reduces the spurious radiation of waves inward through the downstream

boundary, but otherwise has a relatively minor impact on the solution (Fig. 4f). In contrast, in the two-way case the filter substantially reduces the reflection (Fig. 4g) relative to that generated by the unfiltered sponge BC (Fig. 4e).

The magnitude of the reflections produced by the filtered sponge BC is compared with that for the standard sponge BC as a function of wavelength in Fig. 5. For two-way nesting and incident waves that are poorly resolved on the coarse grid ($< 12\Delta x_n$), filtering greatly reduces the reflections. (Compare the black crosses with the open black squares.) At longer wavelengths, the filtered sponge BC also outperforms the unfiltered sponge BC, although the both give very similar results for wavelengths longer than $20\Delta x_n$. In one-way nesting, the improvement produced by filtering is much smaller and is largely limited to wavelengths between 8 and $11\Delta x_n$. (Compare the gray crosses with the open gray diamonds.)

4. Analysis of reflections generated by the interpolation BC

a. One-way nesting

The reflection generated at the nested-grid boundary using one-way nesting is strongly influenced by any difference in the phase of the wave on the coarse and nested grids in the neighborhood of the nested-grid boundary.² Such differences are illustrated for a $24\Delta x_n$ wave in Fig. 6a, in which the coarse- and nested-grid waves from a one-way simulation are both plotted in the region near the original nest boundary, although for these simulations, the actual nest boundary has been moved far beyond the right edge of the plot. Due to numerical dispersion and the difference in resolution of the wave on the coarse and nested grids, the phase speed of the wave on the coarse grid is slower than that on the nested grid.

The difference in numerical phase speeds between the two grids is relatively small for

²Elsberry (1978) noted that reflections in one-way nesting could be caused by the solutions moving out of phase between the two grids, although he did not elaborate on this idea.

the $24\Delta x_n$ wave; however, in the one-way case, the difference in phase accumulates as the waves propagate toward the nested grid boundary, so that for the particular dimensions of the nested grid used here, the coarse and nested solutions are nearly half a wavelength out of phase when the packet arrives at the boundary (Fig. 6a), yielding the maximum amount of reflection. The difference in phase speeds on the coarse and nested grids is larger for a $18\Delta x_n$ wave, yet counterintuitively smaller reflections are produced because for the domain size we are using, the $18\Delta x_n$ waves come back into phase by the time the center of the wave packet reaches the boundary (Fig. 6b). Small reflections nevertheless occur in the $18\Delta x_n$ case because at earlier or later times, when the wave amplitude at the boundary is lower, there is some difference in phase between the solutions on the two grids.

Theoretical estimates for the interpolation BC's errors in one-way nesting can be derived as a function of the computational phase speeds on each grid. If we neglect the amplitude modulation of the wave packet, we can easily determine the reflection r_{1w} produced solely by the phase difference in the carrier wave on each grid. Suppose unit-amplitude monochromatic waves of the same wavelength ($2\pi/k$) are in phase on the coarse and nested grids at time $t = 0$, and assume the interpolation BC is imposed at some point $x = L$ (which we will take to be the boundary of the nested grid). The interpolation BC will generate a reflected wave of amplitude r_{1w} and wavenumber $-k$ on the nested grid, and the matching condition at $x = L$ becomes

$$\exp(ikL - i\omega_n t) + r_{1w} \exp(-ikL - i\omega_n t) = \exp(ikL - i\omega_c t),$$

where $\omega_n(k)$ and $\omega_c(k)$ are the frequencies on the nested and coarse grids as given by the discrete dispersion relation.

Solving for r_{1w} yields:

$$r_{1w} = \exp(i\omega_n t) \exp(2ikL) [\exp(-i\omega_c t) - \exp(-i\omega_n t)],$$

or

$$|r_{1w}| = |\exp(-i\omega_c t) - \exp(-i\omega_n t)|.$$

Using the relationships $\omega_n = c_n k$ and $\omega_c = c_c k$ for the phase speeds c_n and c_c on the nested and coarse grids, the amplitude of the reflected wave being produced at time t may be expressed

$$|r_{1w}| = \sqrt{2} [1 - \cos(k(c_n - c_c)t)]^{1/2}, \quad (9)$$

where, for our staggered grid approximation to the shallow-water equations in the limit of good time resolution ($c\Delta t/\Delta x \ll 1$),

$$c_n = \frac{2c}{k\Delta x_n} \sin\left(\frac{k\Delta x_n}{2}\right) \quad c_c = \frac{2c}{k\Delta x_c} \sin\left(\frac{k\Delta x_c}{2}\right). \quad (10)$$

In our simulations, t is chosen to be the time when center of the nested-grid wave packet reaches the boundary.

b. Two-way nesting

A similar analysis can be performed for two-way nesting. Vichnevetsky (1981) derived the expression

$$r_{2w} = \frac{c_{gn} - c_{gc}}{c_{gn} + c_{gc}} \quad (11)$$

for reflection at a grid refinement as a function of the numerical *group* speeds³ c_{gn} , c_{gc} on the nested and coarse grids, respectively. Since wave propagation back and forth across the nest boundary in a two-way nest is very similar to that for a grid refinement, we will use the same expression as an estimate of the expected reflection amplitude of a unit-amplitude disturbance at the nested-grid boundary when using a two-way nest and the interpolation BC.

³Defined as $\partial\omega/\partial k$, where ω is the frequency from the computational dispersion relation.

The derivation of (11) uses the assumption that the frequencies (not wavenumbers⁴) of the waves on the two grids match; thus, the wavenumber k_c of the coarse-grid solution is that which satisfies

$$c_n k = c_c k_c, \quad (12)$$

where k is the wavenumber on the nested grid which is specified by the initial condition. For the staggered-grid second-order spatial discretization used here, (12) implies

$$\sin\left(\frac{k_c \Delta x_c}{2}\right) = \frac{\Delta x_c}{\Delta x_n} \sin\left(\frac{k \Delta x_n}{2}\right). \quad (13)$$

As the wavelength on the nested grid decreases, the right-hand side of (13) will exceed unity and k_c will become complex-valued, implying that the coarse-grid solution will be evanescent. For $\Delta x_c/\Delta x_n = 3$ evanescence is predicted to occur for nested grid wavelengths $\leq 9\Delta x_n$, although numerical tests show that the longest nested grid wavelength which is transmitted into an evanescent wave is approximately $8.5\Delta x_n$. The coarse-grid solution for this wave is shown in Fig. 7; here, the amplitude of the evanescent disturbance is greatest at 638 s because this is when the center and most intense part of the wave packet arrives at the nested-grid boundary. For all evanescent coarse-grid disturbances, the real part of k_c is $\pi/2$, corresponding to a $2\Delta x_c$ wave. The imaginary part of k_c is smallest, and the e-folding distance on which the wave decays is largest, for a wavelength just short enough to cause evanescence.

We may now use Vichnevetsky's expression (11) for reflections in two-way nesting where, for our discretization, the group velocities are

$$c_{gn} = c \cos\left(\frac{k \Delta x_n}{2}\right) \quad c_{gc} = c \cos\left(\frac{\text{Re}(k_c) \Delta x_c}{2}\right) \quad (14)$$

⁴The solutions in a two-way nested simulation are held identical over the update region (the region where the two grids coincide, sponge zones excepted), and so the coarse-grid wavelength can only change when the solution propagates out of the update region. In contrast, in one-way nesting the coarse-grid solution is initialized to and remains the same wavelength as that on the nested grid.

Note that evanescent coarse-grid solutions have a group velocity of 0, so $r_{2w} = 1$ and we expect total reflection.

c. Comparison with numerical results

The amplitude of the reflections estimated from (9) and (11) are compared with the results from simulations with the interpolation BC in Fig. 3a. Except for waves shorter than $18\Delta x_n$ (which corresponds to a only moderately-resolved $6\Delta x_c$ wave on the coarse grid), the agreement between (9) and the one-way numerical simulations is quite good; and for all wavelengths the agreement between (11) and the two-way numerical simulations is very good. We conclude from this that the reflections in the one-way interpolation case can be interpreted as arising from the differences in the phase of the wave on the coarse and nested grids, and that reflections in the two-way interpolation case arise from differences in the group velocity. In the case of the one-way interpolation BC, the errors in the estimates for shorter wavelengths appear because (9) does not take into account the finite width of the packet. The range of phase differences that occur over the width of the packet increases as the difference between the phase speeds on the coarse mesh increases, which in turn increases as the wavelength of the carrier wave decreases. Although (9) is based solely on the phase difference when the center of the packet reaches the boundary, reasonable qualitative agreement is seen in Fig. 3a down to $15\Delta x_n$ ($5\Delta x_c$), below which the theoretical value becomes highly oscillatory (and so is not plotted). The two-way estimate (11) correctly predicts very small reflections for wavelengths larger than $24\Delta x_n$ ($8\Delta x_c$) and accurately predicts the simulated reflections through the smallest wavelengths, including the total reflection occurring for wavelengths $\leq 9\Delta x_n$.

The difference in the group velocities on the fine and coarse meshes for packets with wavelengths of $9\Delta x_n$ or shorter is large enough that, on a one-way mesh, the nested-grid packet attempts to pass through the boundary before the coarse-grid packet has even arrived. As a consequence, the coarse-grid values imposed at the nest boundary are almost zero, and

the interpolation BC generates almost total reflection. Further, once the coarse-grid solution reaches the nested grid’s boundary, the BC will radiate the coarse-grid solution back onto the nested grid, creating the incoming disturbance seen in Fig. 4b.

d. Implications for the sponge BC

The sponge BC causes lower-amplitude reflections than does the interpolation BC, but for well-resolved wavelengths behaves similarly to the interpolation BC with respect to changes in the solution’s wavelength (Fig. 3): two-way nesting yields small but progressively larger reflections with decreasing wavelength, and one-way nesting has peaks in reflection amplitude at 24 and $16\Delta x_n$ with a local minimum in between. More prominent qualitative differences between the behavior of the two BCs are found for poorly-resolved wavelengths. When using the sponge BC and a one-way nest, wavelengths $\leq 9\Delta x_n$ are damped towards the zero coarse-grid solution, causing the sponge BC to act as a damping layer and thus substantially reducing the amplitude of the reflections. However, much like the interpolation BC the sponge BC creates an incoming disturbance (Fig. 4d) once the coarse-grid solution reaches the nested-grid boundary. This is mitigated by the use of the filtered sponge BC (Fig. 4f), which damps the poorly-resolved coarse-grid data before applying it to the nested-grid solution in the sponge zone.

The high-frequency coarse-grid modes appearing for marginally-well-resolved solutions in two-way nesting can degrade the sponge BC by creating a mismatch in the sponge zone, so that the BC fails to appropriately damp the outgoing nested grid solution. This is particularly pronounced at $9\Delta x_n$ (Fig. 4e), which transmits into a slowly-propagating mode with a wavelength slightly longer than $2\Delta x_c$. This disturbance greatly differs in wavelength from the nested grid solution, while also having a larger amplitude than the evanescent solutions and failing to decay away from the nested-grid boundary. Hence, the $9\Delta x_n$ two-way case causes a coarse-grid solution which interferes the most with the sponge BC and causes the greatest reflection compared to other wavelengths. The effectiveness of the filtered

sponge BC (Figs. 4g, 5) verifies these assertions: if these interfering coarse-grid disturbances are filtered out, the reflections in two-way nested simulations are greatly reduced.

5. Generalizing the preceding results

a. Other finite difference schemes

The formulas (9) and (11) for the amplitudes of reflected waves may also be applied to other numerical schemes and other problems involving wave propagation. For the interpolation BC, the key factor governing reflections on one-way nests is the difference between the phase speeds on the coarse and fine meshes; for two-way nests, the key factor is the difference in group velocities. Both differences are typically smaller on a staggered grid than on an unstaggered mesh. Higher order methods generally give more uniform (and more accurate) approximations to the phase speeds of all but the very shortest waves with wavelengths less than about $3\Delta x$. At least for longer waves, higher order methods also tend to increase the uniformity in the approximation of the group velocity.

As a concrete example, consider how the differences between the phase speeds and group velocities in numerical approximations to the linearized shallow-water system (1)–(2) are influenced by switching between staggered and unstaggered meshes and between second- and fourth-order centered spatial differences. Using second-order spatial differencing on an unstaggered grid yields the scheme

$$\begin{aligned}\delta_{2t}u + g\delta_{2x}h &= 0 \\ \delta_{2t}h + H\delta_{2x}u &= 0.\end{aligned}$$

In the limit of good time resolution ($c\Delta t/\Delta x \ll 1$), the numerical phase speed and group

velocities for this scheme are

$$c_{2U} = \frac{c}{k\Delta x_c} \sin(k\Delta x_c) \quad \text{and} \quad c_{g_{2U}} = c \cos(k\Delta x_c). \quad (15)$$

Fourth-order spatial differencing on an unstaggered grid gives the method

$$\begin{aligned} \delta_{2t}u + g \left(1 - \frac{(\Delta x)^2}{6} \delta_x^2 \right) \delta_{2x}h &= 0 \\ \delta_{2t}h + H \left(1 - \frac{(\Delta x)^2}{6} \delta_x^2 \right) \delta_{2x}u &= 0, \end{aligned}$$

for which (assuming $c\Delta t/\Delta x \ll 1$)

$$c_{4U} = \frac{c}{6k\Delta x} (8 \sin k\Delta x - \sin 2k\Delta x) \quad \text{and} \quad c_{g_{4U}} = \frac{c}{3\Delta x} (4 \cos k\Delta x - \cos 2k\Delta x). \quad (16)$$

Finally, the scheme

$$\begin{aligned} \delta_{2t}u + g \left(1 - \frac{(\Delta x)^2}{24} \delta_x^2 \right) \delta_x h &= 0 \\ \delta_{2t}h + H \left(1 - \frac{(\Delta x)^2}{24} \delta_x^2 \right) \delta_x u &= 0, \end{aligned}$$

is a fourth-order spatial discretization on a staggered grid. In the limit of good time resolution the phase speed and group velocity for this scheme satisfy

$$\begin{aligned} c_{4S} &= \frac{2c}{k\Delta x} \left[\frac{9}{8} \sin \left(\frac{1}{2}k\Delta x \right) - \frac{1}{24} \sin \left(\frac{3}{2}k\Delta x \right) \right] \\ c_{g_{4S}} &= \frac{c}{8} \left[9 \cos \left(\frac{1}{2}k\Delta x \right) - \cos \left(\frac{3}{2}k\Delta x \right) \right]. \end{aligned} \quad (17)$$

In the case of one-way nesting, the actual reflections produced in a specific situation depend on the difference in the phase of the waves on the coarse and fine meshes at the fine-mesh boundary. This is a function of the distance to the boundary as well as the difference in the phase speeds on each mesh. Nevertheless, the larger the difference in the phase

speeds, the more quickly the waves get out of phase and, in general, the larger the reflection that will be produced at a “nearby” boundary. Thus in Fig. 8 we characterize the potential of the preceding schemes to produce reflections by plotting the difference in phase and group velocities between the nested and coarse grids assuming a 3-to-1 grid refinement. In the one-way case (Fig. 8a), the coarse- and fine-mesh waves stay in phase better using staggered meshes and fourth-order schemes.⁵ If for simplicity we neglect the difference in wavenumber between the two grids, the situation for two-way nesting (Fig. 8b) is roughly similar except that there is a much broader range of short waves for which fourth-order unstaggered differencing creates larger group-velocity differences than the second-order unstaggered approach. Numerical simulations have verified that the preceding methods do indeed produce reflections whose amplitudes vary from scheme to scheme in a manner consistent with the phase-speed and group-velocity differences shown in Fig. 8.

Of course the phase speeds and group-velocities are also influenced by the time differencing. Leapfrog time differencing accelerates the phase whereas centered space differencing decelerates the phase. If leapfrog time differencing is combined with second-order centered space differencing on an unstaggered grid, the phase errors in the resulting method tend to cancel, and they approach zero as $c\Delta t/\Delta x \rightarrow 1^-$. For the other three schemes considered in the preceding analysis, the net phase-speed and group velocity errors are more complicated functions of the Courant number and the wavelength, although they could nevertheless be evaluated in specific cases if so desired.

b. Effect of nested grid width

If the width of a *one-way* nested grid is changed, but the initial location of the wave packet is unchanged so that the wave takes a different amount of time to reach the boundary, the difference in phase between the solutions should also change, in which case (9) implies that

⁵The sole exceptions are waves shorter than about $7\Delta x_n$ for which the differences in phase speed for the fourth-order unstaggered scheme exceed those for the second-order unstaggered method.

the amplitude of the reflections should be different. Conversely, we expect that no such sensitivity to the width of the nested grid should be evident in a two-way nest, since the solutions remain in sync and the reflections are due to the changes in group velocity between the grids. To test this, a series of simulations has been performed in which the position of the eastern end of the nested grid is moved. The initial disturbance remains centered in the same location, so the time required for the packet to reach the boundary will be proportional to the width of the domain.

Fig. 9 shows the amplitude of the reflected mode for $24\Delta x_n$ waves in a one-way nest of varying lengths. It is apparent that as the nested grid width changes, the reflection from the interpolation BC varies like a rectified sine wave. The minimum reflections occur where the waves are in phase at the boundary, although as discussed previously, (9) underestimates the actual reflection when the waves are perfectly superimposed because it does not account for the variation in phase that occurs while a wave packet of finite width passes through the boundary. The sponge and filtered sponge BCs greatly reduce the reflection on the one-way nest, with little difference between the two BCs at this wavelength, but still show sensitivity to the relative phases of the coarse and nested-grid waves at the boundary. On the other hand, the reflections generated using two-way nesting are independent of the size of the domain regardless of the BC used, consistent with the insensitivity of (11) to time or position. The two-way example plotted in Fig. 9 uses the interpolation BC; the reflections generated by the sponge or filtered sponge BC on the two-way grid would plot as zeros and are not shown.

The sensitivity of one-way nesting to grid width also extends to shorter wavelengths. The nested grid solution on a 4000 m wide one-way nested grid (not shown) using a $9\Delta x_n$ disturbance no longer outruns the coarse-grid solution, and the reflections are found to be larger than for the original grid width for all three BCs, although the increase is reduced by using the filtered sponge BC. Again, two-way nesting shows little sensitivity to grid width, and if the filtered sponge BC is used two-way nesting yields smaller reflections than one-way

nesting for this grid width.

c. Sensitivity of the Sponge BC

Is the relative performance of one-way and two-way nesting dependent upon the parameters defining the sponge BC? One might suppose that as the sponge zone becomes thicker, any reflection might be sufficiently reduced to the point where one-way and two-way nesting would perform similarly. To address this question, reflection amplitudes for a well-resolved $24\Delta x_n$ wave and a more poorly-resolved $9\Delta x_n$ wave are plotted as a function of the width of the sponge in Fig. 10 for both one-way and two-way nesting. For the $24\Delta x_n$ wave (Fig. 10a), two-way nesting is far superior to one-way nesting for sponge zones of any finite width (zero width corresponds to the interpolation BC), with the results differing little between the sponge or the filtered sponge BC. Indeed, the reflection on the one-way nest using a 15-point sponge is an order of magnitude larger than that on the two-way nest with only a three-point sponge. With the WRF default of three sponge points, the one-way nest yields a reflection almost a third of the size of the incident disturbance, while the two-way nest reduces the amplitude of the reflected mode to less than 1%.

As shown in Fig. 10b, the sponge BC performs poorly when a $9\Delta x_n$ wave encounters the boundary of a two-way nest. Somewhat better results may be achieved using the conventional sponge BC in a one-way nest, but much better results are obtained using the filtered sponge BC. The two-way filtered sponge BC generates less reflection than the other configurations except for very wide sponges where the reflections are negligible (note the logarithmic vertical scale).

We may also examine changing the sponge weight W in (5). If the weight is too small the BC would not effectively absorb the outgoing waves, while if it is too strong the BC would itself create reflections. Furthermore, since the coefficients are inversely proportional to Δt , taking a shorter timestep applies more damping over a given physical time and will thus alter the reflections off of the boundary. This line of thinking suggests that reflections should be

dependent upon $W/\Delta t$, the rate at which the solution in the sponge zone is relaxed to that on the coarse grid. A series of tests were performed in which either W or the timestep were varied so that $W/\Delta t$ was modified from its original value of 0.25 s^{-1} to values in the range of 5×10^{-3} to 2.5 s^{-1} . For wavelengths in the range 18 to $36\Delta x_n$ (in which the filtered and sponge BCs yield nearly identical results) these tests found that two-way nesting still yielded smaller reflections than did one-way nesting for all cases, and for all but the smallest values of this ratio the amplitude of the reflection for two-way nesting was lower by an order of magnitude or more than that using one-way nesting. Similar tests for a $9\Delta x_n$ wave found that both nesting strategies yielded similar reflections when the filtered sponge BC was used regardless of the value of $W/\Delta t$.

6. Conclusion

Numerical dissipation can effectively remove reflections at a nested boundary in problems like scalar advection, where the only waves that can propagate backwards off the boundary are very poorly resolved. However in many physically significant applications well-resolved signals can propagate in both directions across the grid, and in such cases dissipation cannot be relied on to remove the reflected wave unless that dissipation is strong enough to also remove other physically-important waves. Our focus has, therefore, been on a simple system that supports waves that move in different directions: the one-dimensional linearized shallow-water equations. We compared the relative performance of one-way and two-way nesting in transmitting waves through the nested grid boundary. For boundary conditions at the edge of the nest, we tested both simple interpolation and a sponge layer similar to that used in some modern mesoscale models such as WRF.

For moderately-well-resolved solutions on the coarse grid—which were very well-resolved on the nested grid—two-way nesting was found to yield substantially smaller reflections than did one-way nesting. This result was found to be robust to the choice of BC and the

formulation thereof. On a one-way nest, the sponge BC gave the least reflection, but even a very wide 15-point sponge layer still produced much more reflection for these well-resolved solutions.

The two-way nesting strategy keeps the solution on the coarse and nested grids in phase, allowing more consistent coarse-grid fields to be supplied to the nested-grid BC so that well-resolved disturbances are able to exit the nested domain with only minor reflections. These reflections are found to be related to the difference in computational group velocities between the two grids, which increases with decreasing wavelength. In contrast, the solutions on each grid in a one-way nest need not remain in phase and significant differences may develop between the two grids. As a result, the data provided to the boundary conditions from the coarse grid need not match the solution on the one-way nested grid, and nontrivial reflections typically occur. Even small differences in the numerical phase speeds between waves on the coarse and nested grids can gradually accumulate so that when a disturbance reaches the one-way nest's boundary, there is a significant difference between its phase on each grid.

Different behaviors occur if the coarse-grid solution is poorly-resolved. For short-wavelength localized disturbances, the two solutions in a *one-way* simulation may propagate at such different group velocities that the nested-grid solution can reach the nested-grid boundary well before the coarse-grid solution does, so that the coarse-grid solution is zero as the nested grid solution exits. This causes total reflection if the interpolation BC is used, but increases the effectiveness of the sponge BC as it becomes a wave-absorbing layer which damps the nested-grid solution to zero.

For *two-way* nesting, a marginally-resolved nested-grid solution is transmitted onto the coarse grid as either a shorter wavelength propagating mode or an evanescent mode with zero group velocity. In these cases, the reflection is total when using the interpolation BC, and the reflections for the sponge BC are greatly increased as the presence of an inconsistent coarse-mesh solution in the sponge zone interferes with the absorption of the outgoing waves. This problem may be rectified by spatially filtering the coarse grid data supplied to the sponge,

thereby attenuating any short-wavelength coarse-grid disturbances. Adding this filter to the sponge BC modestly decreases the reflections on a one-way nest, and greatly reduces them on a two-way nest.

These results suggest that in our idealized tests, two-way nesting is preferred to one-way nesting given its superiority for well-resolved waves, and that it is no worse than one-way nesting for poorly-resolved solutions if a filter is added to the sponge BC. Unsurprisingly, the sponge and filtered sponge BCs are seen to uniformly produce smaller reflections than does the interpolation BC.

A key remaining question is how directly these results extend to more realistic simulations. A forthcoming paper will examine the difference between the two nesting strategies in meteorologically-relevant flows and propose guidance to modelers.

Acknowledgements: This research was supported by NSF grant ATM-0836316. The authors thank two anonymous reviewers for their comments which greatly improved this paper.

REFERENCES

- Carpenter, K., 1982: Note on the paper, Radiation conditions for lateral boundaries of limited area numerical models. *QJR Meteorol. Soc*, **110**, 717–719.
- Clark, T. and R. Farley, 1984: Severe Downslope Windstorm Calculations in Two and Three Spatial Dimensions Using Anelastic Interactive Grid Nesting: A Possible Mechanism for Gustiness. *J. Atmos. Sci*, **41** (3), 329–350.
- Colle, B., J. Wolfe, W. Steenburgh, D. Kingsmill, J. Cox, and J. Shafer, 2005: High-Resolution Simulations and Microphysical Validation of an Orographic Precipitation Event over the Wasatch Mountains during IPEX IOP3. *Mon. Wea. Rev.*, **133** (10), 2947–2971.

- Davies, H., 1976: A lateral boundary formulation for multi-level prediction models. *Quarterly Journal of the Royal Meteorological Society*, **102 (432)**, 405–418.
- Deng, X. and R. Stull, 2005: A Mesoscale Analysis Method for Surface Potential Temperature in Mountainous and Coastal Terrain. *Mon. Wea. Rev.*, **133 (2)**, 389–408.
- Durrán, D., 1991: The third-order Adams-Bashforth method: An attractive alternative to leapfrog time differencing. *Monthly Weather Review*, **119 (3)**, 702–720.
- Durrán, D., 1999: *Numerical Methods for Wave Equations in Geophysical Fluid Dynamics*. Springer.
- Elsberry, R., 1978: Prediction of atmospheric flows on nested grids. *Computational Techniques for Interface Problems*, K. C. Park and D. K. Gartling, Eds., American Society of Mechanical Engineers, No. 30 in Applied Mechanics Division, 67–86.
- Giorgi, F. and L. Mearns, 1999: Regional climate modeling revisited: an introduction to the special issue. *J. Geophys. Res.*, **104 (D6)**, 6335–6352.
- Knievel, J., G. Bryan, and J. Hacker, 2007: Explicit numerical diffusion in the WRF Model. *Monthly Weather Review*, **135 (11)**, 3808–3824.
- Krol, M., et al., 2005: The two-way nested global chemistry-transport zoom model TM5: algorithm and applications. *Atmos. Chem. Phys.*, **5**, 417–432.
- Mar-Or, A. and D. Givoli, 2006: The global-regional model interaction problem-analysis of carpenter’s scheme and related issues. *Int. J. Multiscale Comput. Eng. v4*, 617–646.
- Mass, C., D. Ovens, K. Westrick, and B. Colle, 2002: Does increasing horizontal resolution produce more skillful forecasts? the results of two years of real-time numerical weather prediction over the pacific northwest. *Bull. Amer. Meteor. Soc.*, **83**, 407–430.

- Moeng, C., J. Dudhia, J. Klemp, and P. Sullivan, 2007: Examining Two-Way Grid Nesting for Large Eddy Simulation of the PBL Using the WRF Model. *Monthly Weather Review*, **135** (6), 2295–2311.
- Phillips, N. and J. Shukla, 1973: On the Strategy of Combining Coarse and Fine Grid Meshes in Numerical Weather Prediction. *J. Appl. Meteor.*, **12** (5).
- Skamarock, W. and J. Klemp, 1993: Adaptive grid refinement for two-dimensional and three-dimensional nonhydrostatic atmospheric flow. *Mon. Wea. Rev.*, **121**, 788–804.
- Skamarock, W., J. Klemp, J. Dudhia, D. Gill, D. Barker, W. Wang, and J. Powers, 2005: A description of the Advanced Research WRF Version 2. *NCAR Tech Notes-468+ STR*.
- Staniforth, A., 1997: Regional modeling: A theoretical discussion. *Meteorol. Atmos. Phys.*, **63**, 15–29.
- Sundstrom, A. and T. Elvius, 1979: Computational problems related to limited area modelling. *Numerical Methods Used in Atmospheric Models*, **2**, 379–416.
- Vichnevetsky, R., 1981: Propagation through numerical mesh refinement for hyperbolic equations. *Math. Comput. Simulation*, **23**, 344–353.
- Warner, T., R. Peterson, and R. Treadon, 1997: A tutorial on lateral boundary conditions as a basic and potentially serious limitation to regional numerical weather prediction. *Bull. Amer. Meteor. Soc.*, **78** (11), 2599–2617.
- Zhang, D.-L., H.-R. Chang, N. L. Seaman, T. Warner, and J. Fritsch, 1986: A two-way interactive nesting procedure with variable terrain resolution. *Mon. Wea. Rev.*, **114**, 1330–1339.

List of Tables

- 1 Selected forecast mesoscale models and their nesting methodology. *For the Washington, D.C. forecast area; Gulf of Mexico and San Francisco forecast areas use slightly different nesting methodologies and lower resolutions, but still use one-way nesting. Recent real-time hurricane simulations with COAMPS-OS use two-way nesting. **RAMS no longer operational at the time of writing. 29
- 2 Reflection amplitudes for various initial conditions and BCs in the 1D shallow-water model. Simulations use no damping of the form (7) unless otherwise specified. 30

Organization	Model	Resolutions	Method
Washington	WRF	36, 12, and 4 km	One-way
Wisconsin	UW-NMS	160, 80, and 27 km	Two-way
Oklahoma	ARPS/wx	27, 9, and 3 km	One-way
NCAR AMPS	WRF	45, 15, 5, and 1.7 km	Both
NCAR Real-time	WRF	36 and 12 km	Two-way
Penn State	WRF	36, 12, 4, 1.33 and 0.44 km	One-way
NRL	COAMPS-OS	27, 9, 3, and 1 km*	One-way
Colorado State	RAMS**	48, 12, and 3 km	Two-way
FSL	RUC-HRRR	13 and 3 km	One-way

TABLE 1. Selected forecast mesoscale models and their nesting methodology. *For the Washington, D.C. forecast area; Gulf of Mexico and San Francisco forecast areas use slightly different nesting methodologies and lower resolutions, but still use one-way nesting. Recent real-time hurricane simulations with COAMPS-OS use two-way nesting. **RAMS no longer operational at the time of writing.

IC Wavelength	Interpolation BC		Sponge BC	
	One-way	Two-way	One-way	Two-way
$36\Delta x_n$	76%	2.4%	8.5%	0.02%
$24\Delta x_n$	186%	5.4%	20.%	0.38%
$18\Delta x_n$	90.%	10.%	9.9%	0.94%
$36\Delta x_n, \gamma_4 = 0.1$	47%	2.1%	7.3%	0.18%
$9\Delta x_n$	107%	96%	19%	44%

TABLE 2. Reflection amplitudes for various initial conditions and BCs in the 1D shallow-water model. Simulations use no damping of the form (7) unless otherwise specified.

List of Figures

- 1 Nested-grid solutions for $h(x, t)$ in simulations of the 1D shallow-water model. (a) shows the initial condition (thin solid line) which is an eastward-propagating $36\Delta x_n$ wave packet. (b)–(e) depict the solution at $t = 1250$ s after any reflection has returned to the center of the nested grid. Interpolation BC results are shown for one-way (b) and two-way nesting (c). Sponge BC results for one-way nesting are in (d) and two-way nesting in (e). Results from one-way nesting are shown in gray. 34
- 2 Simulation of a $36\Delta x_n$ wave in the scalar advection equation with a one-way nest and the interpolation BC. (a) Initial condition; (b) at $t = 1300$ s, no dissipation; (c) at $t = 1300$ s with fourth-order dissipation applied, $\gamma_4 = 0.01$. The thickness of the line in (b) obscures the $2\Delta x_n$ wavelength of the reflected mode. 35
- 3 One-way vs. two-way nesting in the 1D shallow-water model at time 1200 s. (a): normalized reflection amplitude (8) as a function of wavelength for the interpolation BC; (b) for the sponge BC. Note change in vertical scale in (b) and change in horizontal scale in both panels at $24\Delta x_n$. Solid lines in (a) refer to the estimates (9) and (11) for the reflection amplitudes. 36
- 4 As in Fig. 1, but for a $9\Delta x_n$ wave. Panels (f) and (g) show results using the filtered sponge BC described in Section 3c. 37
- 5 Comparison of normalized reflection amplitudes for the sponge BC with and without filtering. 38

- 6 Nested- (gray) and coarse-grid (black) solutions for simulations in which the eastern boundary of the nest is moved from 11 to 15 km. (a) $24\Delta x_n$ and (b) $18\Delta x_n$ waves at $t = 600$ s, at which time the fine-mesh wave packet is centered around the previous location of the nested-grid boundary (indicated by the heavy vertical line at $x = 11$ km.) 39
- 7 Coarse-grid two-way nested solutions at various times for a $8.5\Delta x_n$ wave. Left edge of plot represents first point on coarse grid which is not updated to from the nested grid. Horizontal tick interval is one coarse-grid interval; vertical tick interval is 1 m, with elongated marks representing 0. 40
- 8 Difference between the nested- and coarse-grid (a) phase and (b) group velocities for several numerical schemes and grid setups, presuming a 3-to-1 grid refinement: second-order in space on a staggered grid (2S; Eqns. 10, 14), second-order in space on an unstaggered grid (2U; Eqn. 15), fourth-order in space on an unstaggered grid (4U; Eqn. 16), and fourth-order in space on a staggered grid (4S; Eqn. 18). Speeds are computed in the limit of good time resolution. Here, c is the true shallow-water wave speed \sqrt{gH} . In (b) the group-speed difference for 4U exceeds unity for coarse-grid wavelengths shorter than $8\Delta x_n$. 41
- 9 Same as Fig. 3, but as a function of the width of the nested grid for a disturbance of wavelength $24\Delta x_n$. The solid line is the estimate (9) for the reflection in the one-way case. One-way reflection amplitudes for the sponge BC (not shown) are nearly identical to those for the filtered sponge BC. 42

10 Same as Fig. 3, but as a function of the number of sponge points for disturbances of wavelengths 24 and $9\Delta x_n$. Reflection amplitudes below 8×10^{-3} are not shown. Note the logarithmic scale on the vertical axis.

43

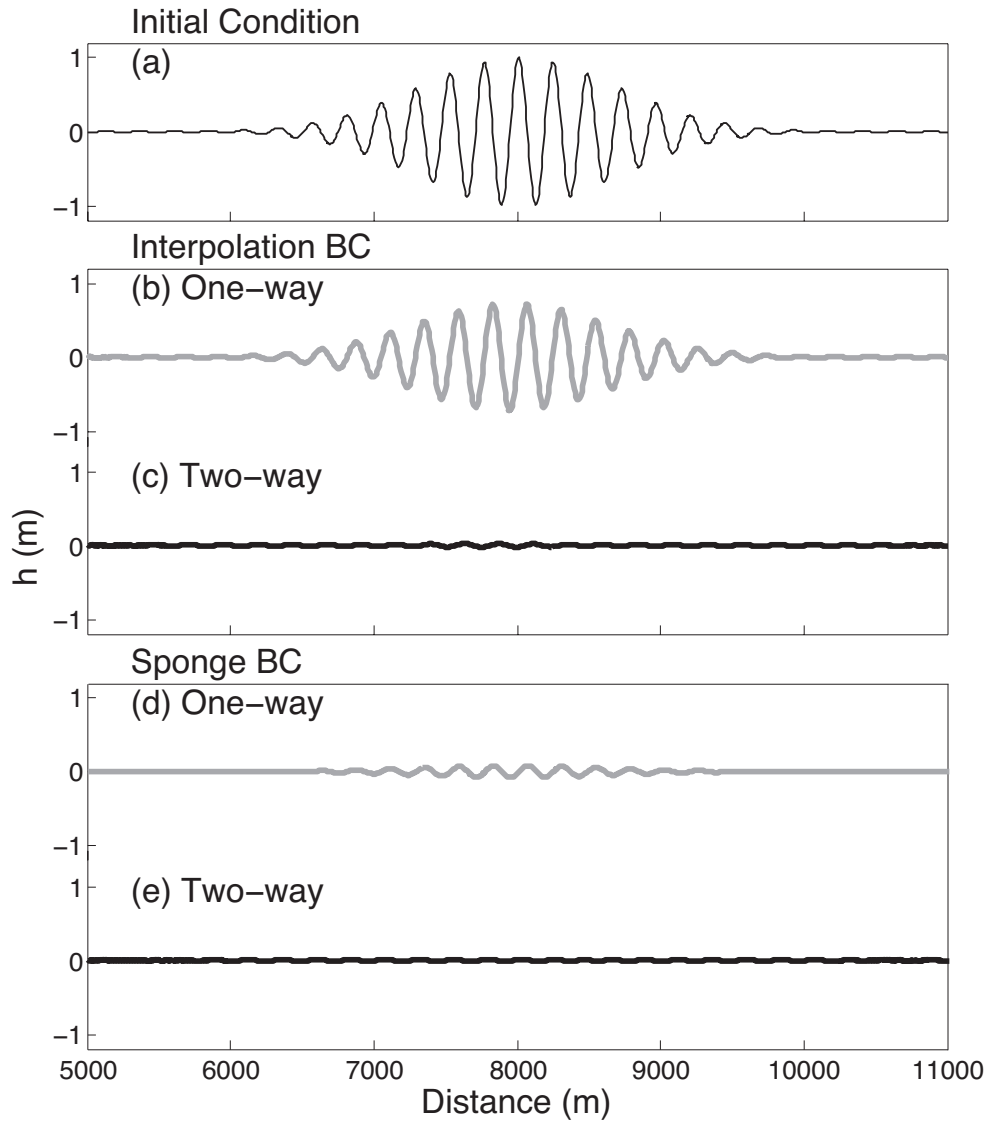


FIG. 1. Nested-grid solutions for $h(x, t)$ in simulations of the 1D shallow-water model. (a) shows the initial condition (thin solid line) which is an eastward-propagating $36\Delta x_n$ wave packet. (b)–(e) depict the solution at $t = 1250$ s after any reflection has returned to the center of the nested grid. Interpolation BC results are shown for one-way (b) and two-way nesting (c). Sponge BC results for one-way nesting are in (d) and two-way nesting in (e). Results from one-way nesting are shown in gray.

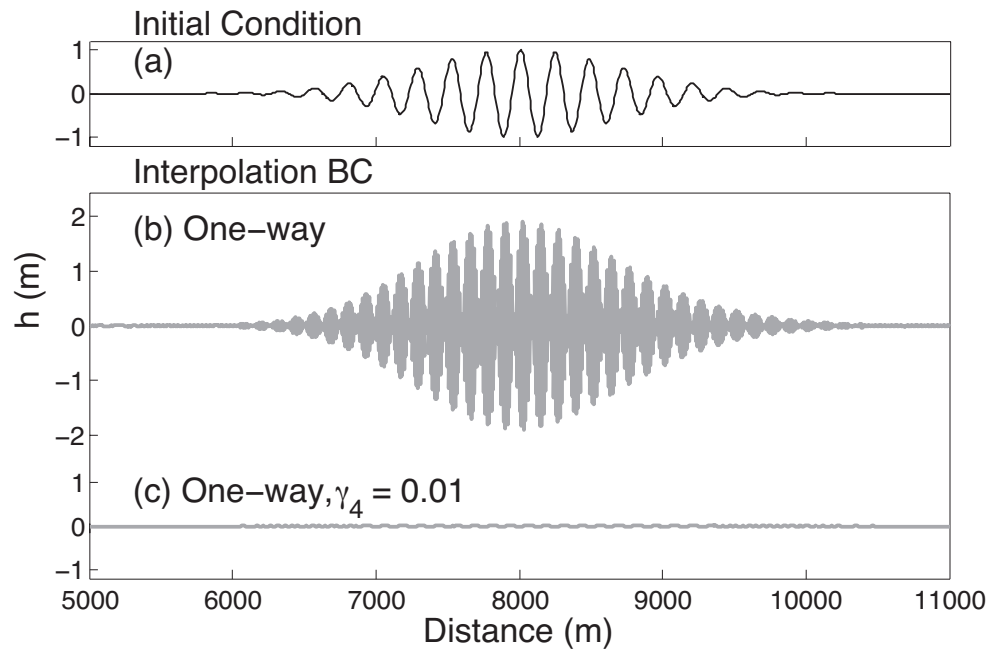


FIG. 2. Simulation of a $36\Delta x_n$ wave in the scalar advection equation with a one-way nest and the interpolation BC. (a) Initial condition; (b) at $t = 1300$ s, no dissipation; (c) at $t = 1300$ s with fourth-order dissipation applied, $\gamma_4 = 0.01$. The thickness of the line in (b) obscures the $2\Delta x_n$ wavelength of the reflected mode.

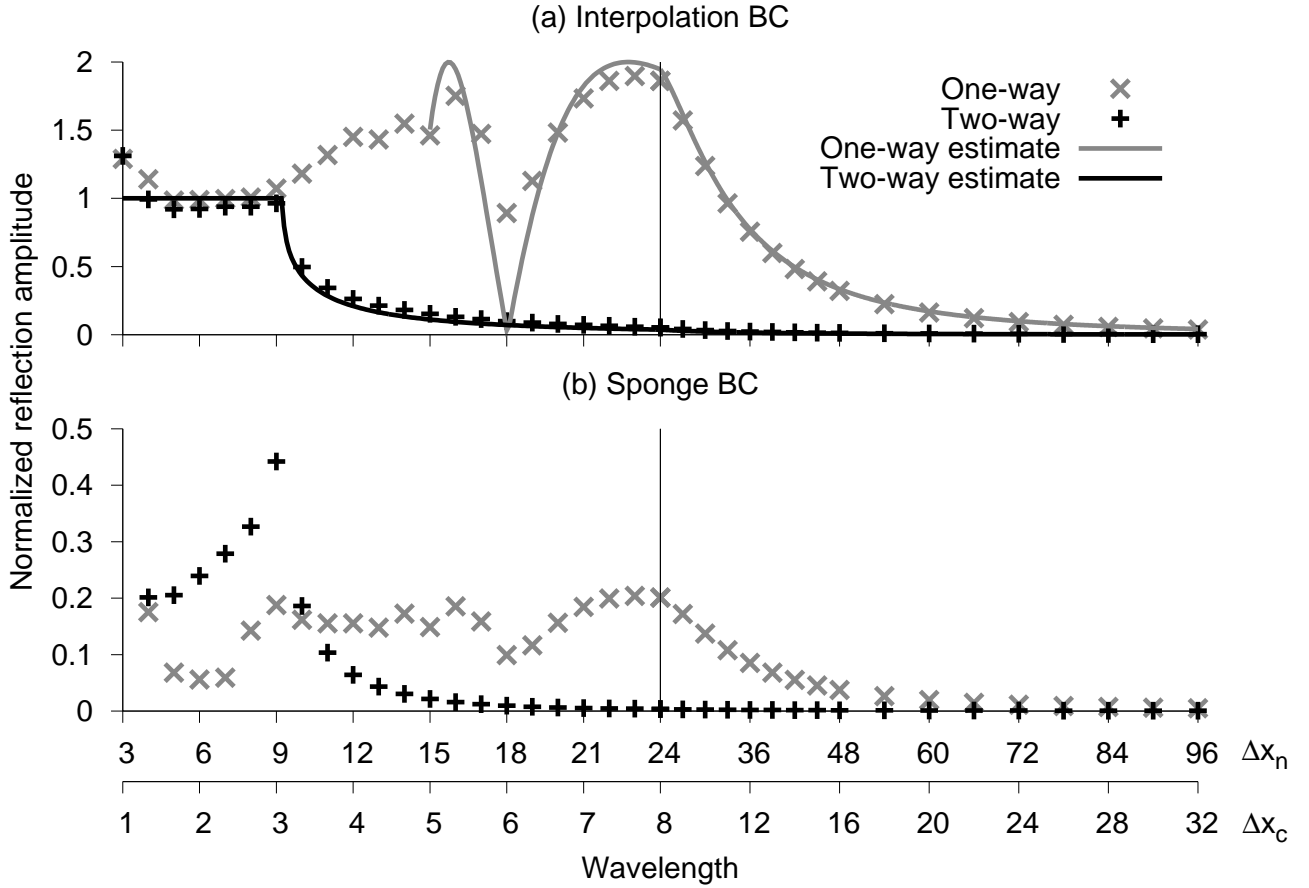


FIG. 3. One-way vs. two-way nesting in the 1D shallow-water model at time 1200 s. (a): normalized reflection amplitude (8) as a function of wavelength for the interpolation BC; (b) for the sponge BC. Note change in vertical scale in (b) and change in horizontal scale in both panels at $24\Delta x_n$. Solid lines in (a) refer to the estimates (9) and (11) for the reflection amplitudes.

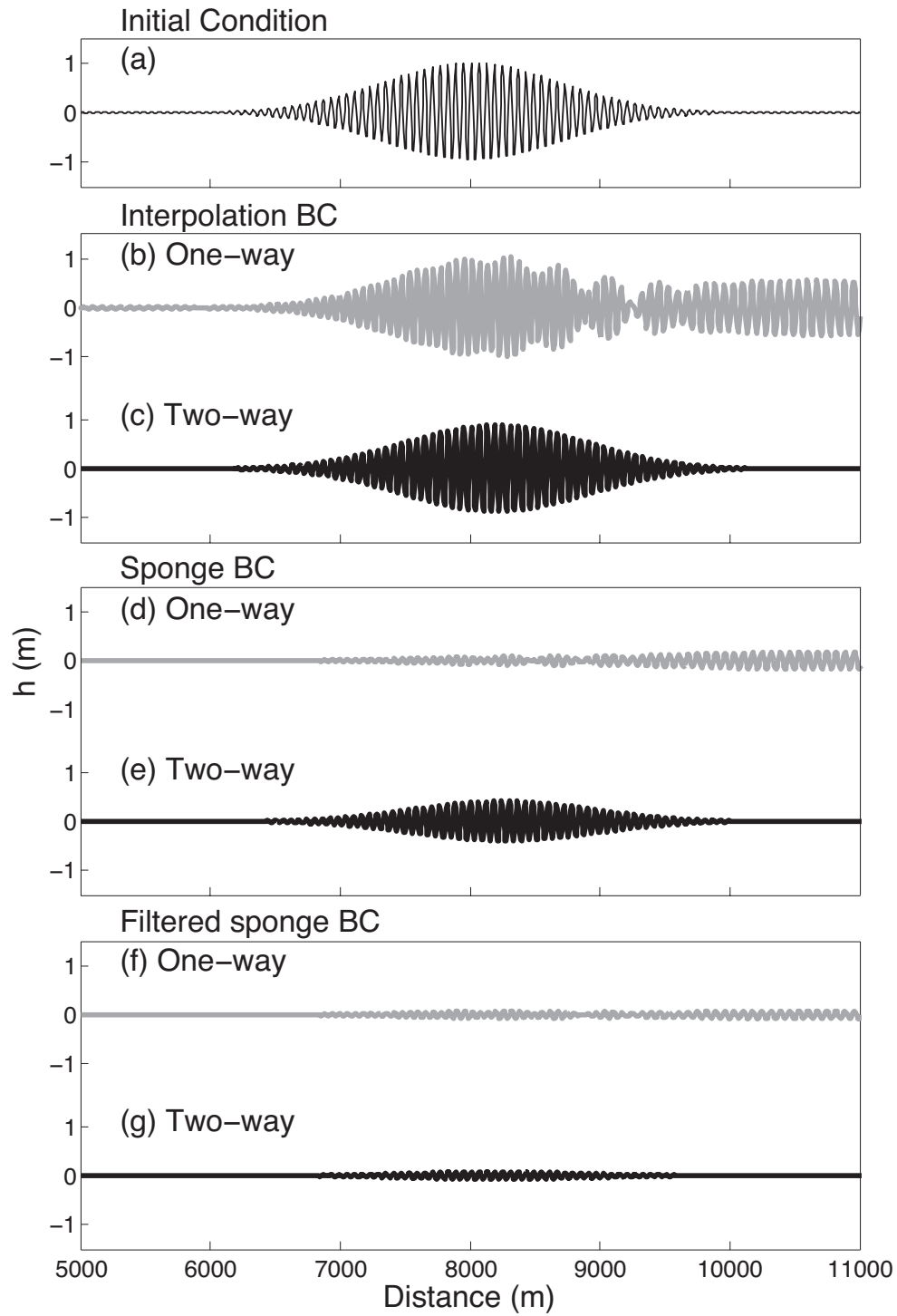


FIG. 4. As in Fig. 1, but for a $9\Delta x_n$ wave. Panels (f) and (g) show results using the filtered sponge BC described in Section 3c.

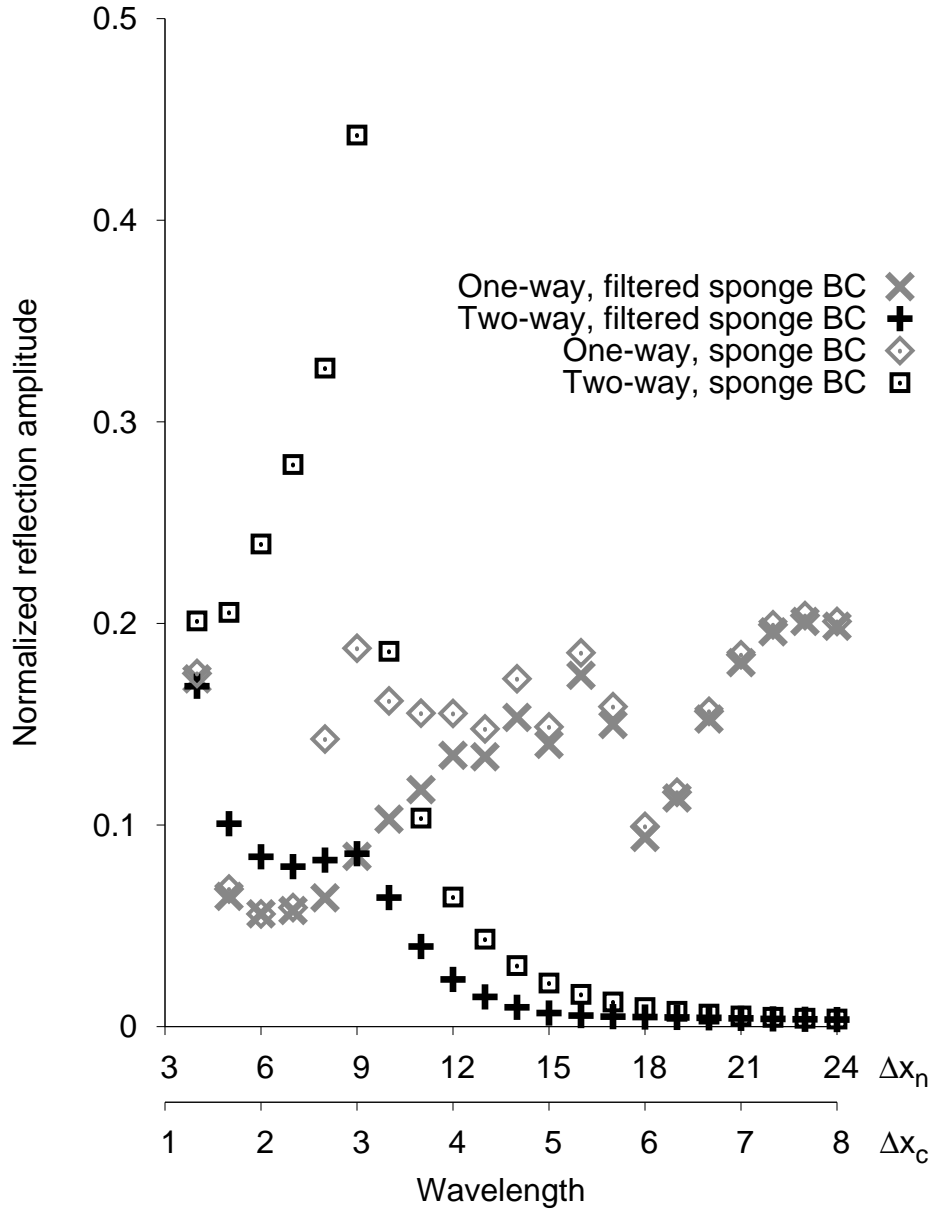


FIG. 5. Comparison of normalized reflection amplitudes for the sponge BC with and without filtering.

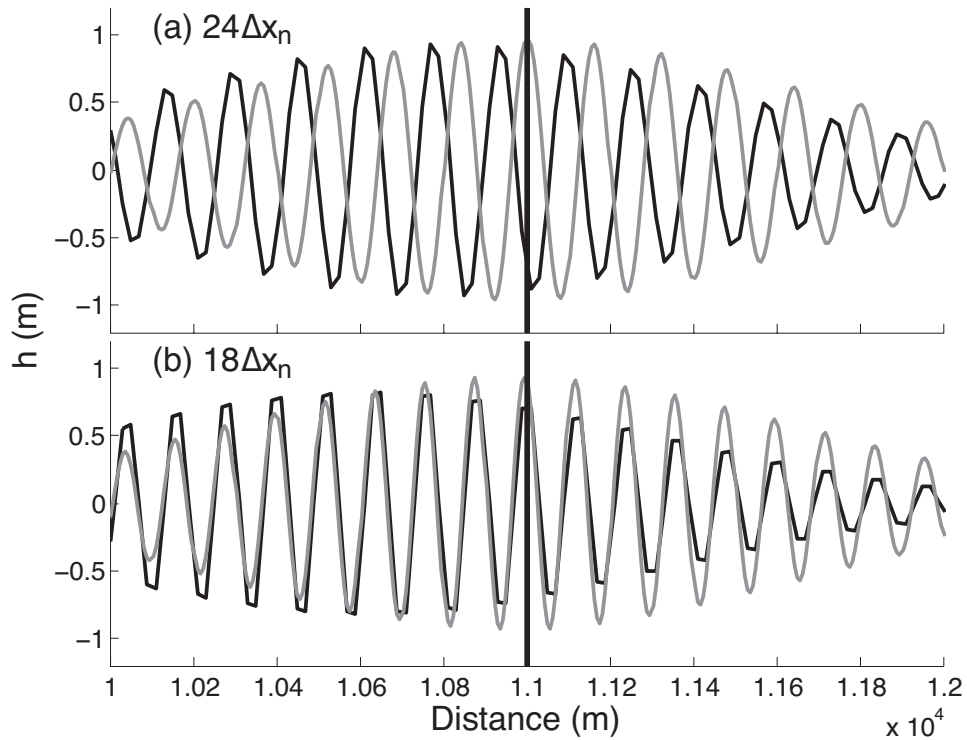


FIG. 6. Nested- (gray) and coarse-grid (black) solutions for simulations in which the eastern boundary of the nest is moved from 11 to 15 km. (a) $24\Delta x_n$ and (b) $18\Delta x_n$ waves at $t = 600$ s, at which time the fine-mesh wave packet is centered around the previous location of the nested-grid boundary (indicated by the heavy vertical line at $x = 11$ km.)

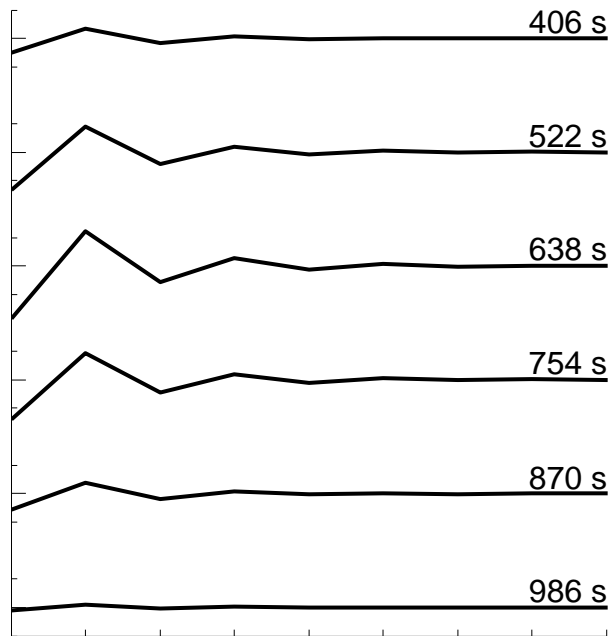


FIG. 7. Coarse-grid two-way nested solutions at various times for a $8.5\Delta x_n$ wave. Left edge of plot represents first point on coarse grid which is not updated to from the nested grid. Horizontal tick interval is one coarse-grid interval; vertical tick interval is 1 m, with elongated marks representing 0.

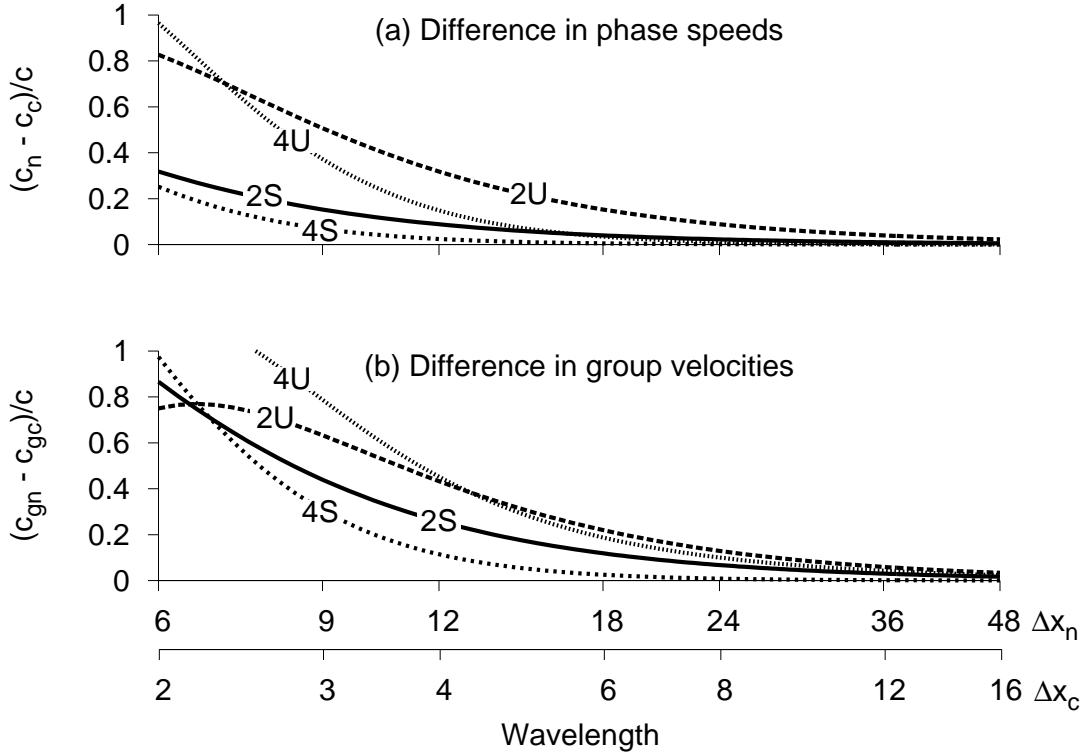


FIG. 8. Difference between the nested- and coarse-grid (a) phase and (b) group velocities for several numerical schemes and grid setups, presuming a 3-to-1 grid refinement: second-order in space on a staggered grid (2S; Eqns. 10, 14), second-order in space on an unstaggered grid (2U; Eqn. 15), fourth-order in space on an unstaggered grid (4U; Eqn. 16), and fourth-order in space on a staggered grid (4S; Eqn. 18). Speeds are computed in the limit of good time resolution. Here, c is the true shallow-water wave speed \sqrt{gH} . In (b) the group-speed difference for 4U exceeds unity for coarse-grid wavelengths shorter than $8\Delta x_n$.

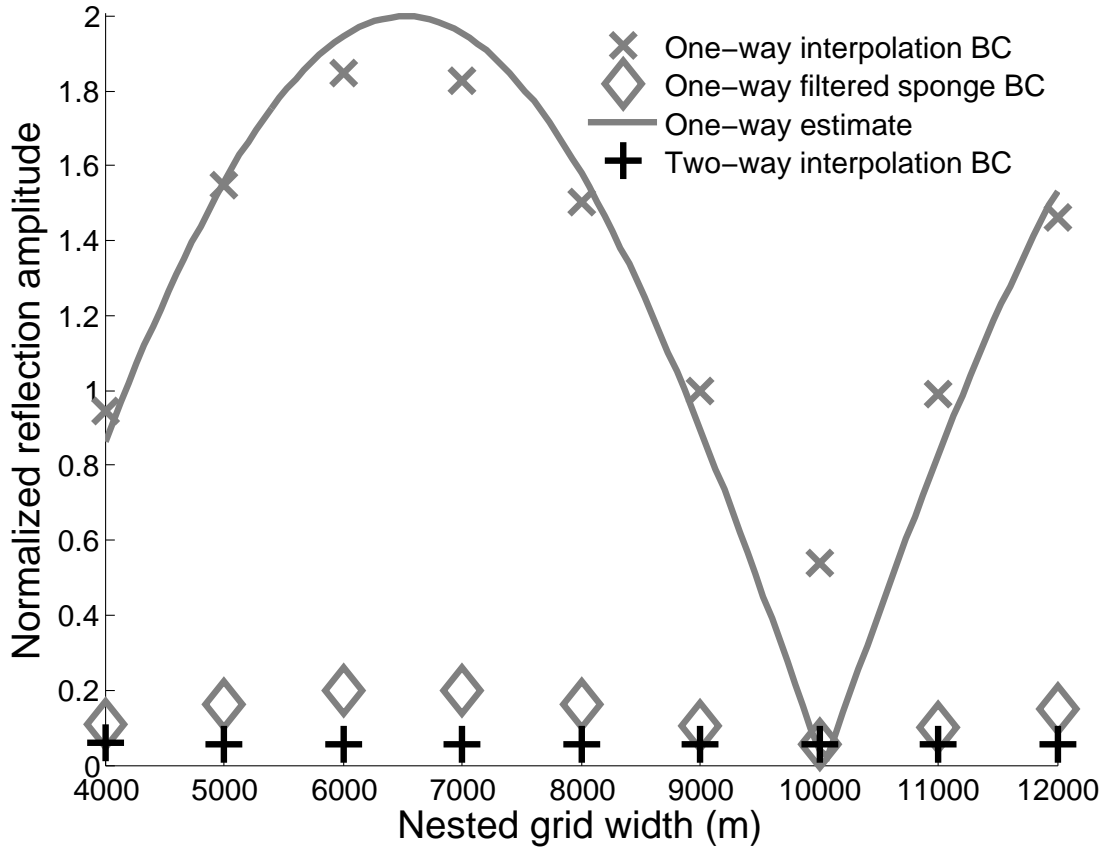


FIG. 9. Same as Fig. 3, but as a function of the width of the nested grid for a disturbance of wavelength $24\Delta x_n$. The solid line is the estimate (9) for the reflection in the one-way case. One-way reflection amplitudes for the sponge BC (not shown) are nearly identical to those for the filtered sponge BC.

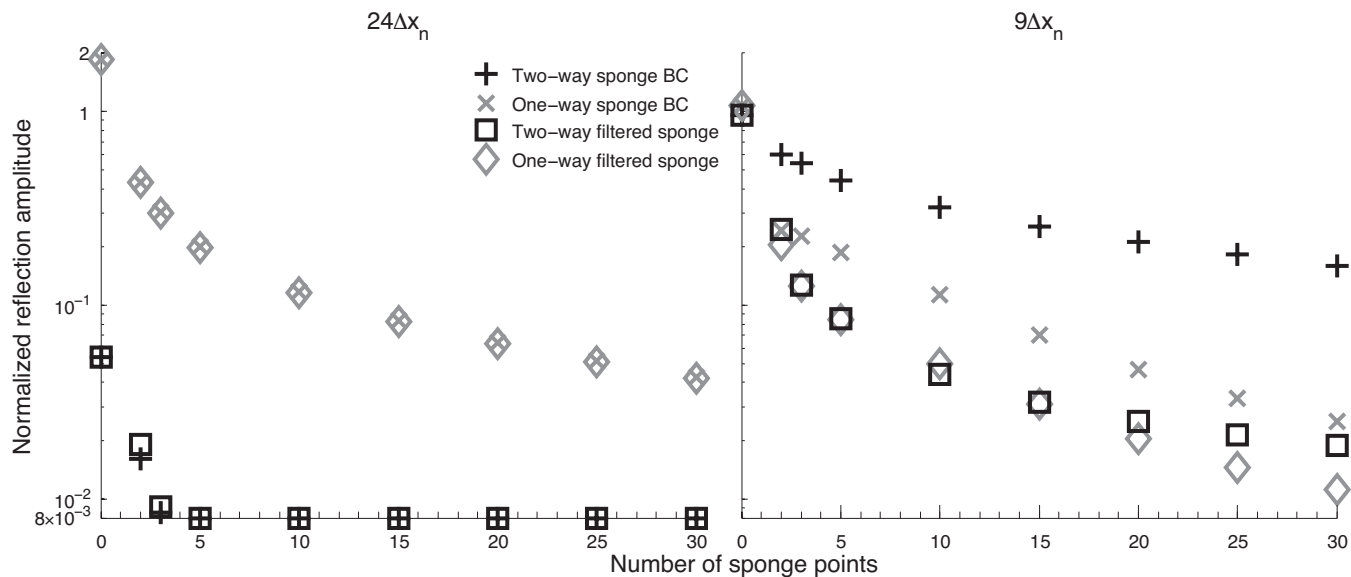


FIG. 10. Same as Fig. 3, but as a function of the number of sponge points for disturbances of wavelengths 24 and $9\Delta x_n$. Reflection amplitudes below 8×10^{-3} are not shown. Note the logarithmic scale on the vertical axis.